



City Research Online

City, University of London Institutional Repository

Citation: Gomez Santos, E., Shi, J., Gavaises, M., Soteriou, C., Winterbourn, M. & Bauer, W. (2020). Investigation of cavitation and air entrainment during pilot injection in real-size multi-hole diesel nozzles. *Fuel*, 263, 116746. doi: 10.1016/j.fuel.2019.116746

This is the preprint version of the paper.

This version of the publication may differ from the final published version.

Permanent repository link: <https://openaccess.city.ac.uk/id/eprint/23265/>

Link to published version: <https://doi.org/10.1016/j.fuel.2019.116746>

Copyright: City Research Online aims to make research outputs of City, University of London available to a wider audience. Copyright and Moral Rights remain with the author(s) and/or copyright holders. URLs from City Research Online may be freely distributed and linked to.

Reuse: Copies of full items can be used for personal research or study, educational, or not-for-profit purposes without prior permission or charge. Provided that the authors, title and full bibliographic details are credited, a hyperlink and/or URL is given for the original metadata page and the content is not changed in any way.

Investigation of cavitation and air entrainment during pilot injection in real-size multi-hole diesel nozzles

Eduardo Gomez Santos^{a,c}, Junmei Shi^{a,*}, Manolis Gavaises^c,
Celia Soteriou^b, Mark Winterbourn^b, Wolfgang Bauer^d

^a*Delphi Technologies, Avenue de Luxembourg, 4940 Bascharage, Luxembourg*

^b*Delphi Technologies, Courteney Rd, Gillingham ME8 0RU, UK*

^c*City, University of London, Northampton Square, London EC1V 0HB, UK*

^d*ANSYS Germany GmbH, Staudenfeldweg 20, 83624 Otterfing, Germany*

Abstract

This paper investigates the complex multiphase flow developing inside the micro-orifices of diesel injector nozzles during pilot injection. High speed micro-visualisations of a transparent serial production nozzle tip replica are used to record the multiphase flow inside the flow orifices as well as near-nozzle spray development. The physical processes taking place are explained with the aid of a three-phase homogeneous mixture model utilized in the context of Large Eddy Simulations. Phase-change due to cavitation is modelled with a Rayleigh-Plesset equation based model, while compressibility of all the phases is considered. Numerical simulations shed light on the interaction between the vortex flow, liquid inertia and cavitation formation that take place simultaneously with air entrainment from the surrounding environment into the injector's sac volume during the injection and the dwell

*Corresponding author

Email address: junmei.shi@delphi.com (Junmei Shi)

time between successive injections. The experimentally observed flow phenomena are well captured by the simulation during all injection phases. In particular the compression of pre-existing air bubbles inside the injector's sac volume during the injector opening, cavitation vapor condensation and air suction after the needle closure are well reproduced.

Keywords: LES, Multiphase flow, Cavitation, Fuel Injection, Realistic nozzle tip visualisation

1. Introduction

New European Real Driving Emission (RDE) driving cycle legislations require significant research efforts to develop emission compliant and efficient passenger car engines [1]. In this context, the so-called digital injection schemes, used to split the fuel injection into multiple small injections with close separation among them, are widely applied in modern diesel engines in order to obtain simultaneous reductions in noise and emissions without compromising engine performance and fuel consumption [2, 3]. Although the nozzle flow for static needle lift conditions has been extensively investigated (see selectively [4, 5, 6, 7]), not much work is available for the flow development during the dynamic operation of the injector, which plays a key influence on emissions [8, 9].

The digital injection schemes are often operated with fast injector needle opening and closing and with very small separation between injections; with typical dwell time of the order of $50\mu s$. This results in highly transient flow

Nomenclature

α_{air}	air volume fraction	[-]	D	injection hole diameter	[m]
α_{liq}	liquid fuel volume fraction	[-]	E	total energy	[J/kg]
α_{nuc}	nuclei content	[-]	F_{vap}, F_{cond}	empirical constants	[m^{-1}]
α_{vap}	vapor fuel volume fraction	[-]	p	pressure field	[Pa]
\mathbf{v}	velocity field	[m/s]	R	gas constant	[J/kg/K]
λ_g	Taylor length scale	[m]	R_b	bubble radius	[m]
μ	viscosity	[Pa s]	R_e, R_c	evaporation/condensation rate	[$kg/m^3/s$]
μ_t	turbulent viscosity	[Pa s]	Re	Reynolds number	[-]
ρ	density	[kg/m^3]	T	temperature	[K]
ρ_{vap}, ρ_{air}	vapour/air density	[kg/m^3]	y^+	non-dimensional wall distance	[-]
σ	viscous stress tensor	[Pa]			
τ_t	turbulent stresses	[Pa]			

16 and formation of massive cavitation inside the injection nozzle. In addition,
 17 modern diesel engines are operated under high injection pressure ($> 2500bar$)
 18 and utilise injectors with small injection hole diameters ($90 - 120\mu m$); these
 19 conditions pose significant difficulties in measuring and/or optically visual-
 20 ising the processes occurring in both the injector nozzle and within the high
 21 temperature combustion chamber. The majority of transparent real-size noz-
 22 zle investigations featuring simplified single-hole geometries that generally
 23 confirm the presence of geometric-induced cavitation [10, 11, 12]. The work
 24 of [13, 14, 15], and the relevant early modelling work [16] were the first to

25 substitute one of the holes of a production nozzle with a quartz window of
 26 identical geometric characteristics and was an experimental breakthrough
 27 that provided valuable information on flow and cavitation structures inside
 28 such micro-channels under realistic operating conditions; further studies were
 29 reported in [17]. A step forward was realised in [18], where a 3-hole, real-
 30 size, fully transparent nozzle allowed for unobstructed optical access inside
 31 the sac volume. Vortex cavitation is dramatically enhanced by vapour or air
 32 already present inside the nozzle volume [19]. Moreover, [20] showed that
 33 the structure of a vortex core is significantly affected by entrained vapour
 34 bubbles. Similarly, [21] demonstrated possible fragmentation of the vortex
 35 core so as to increase the vorticity at the core centre. Finally, the strong in-
 36 teraction observed between vortex properties and bubble dynamics[22], the
 37 coupling of radial and axial growth of bubbles trapped in vortices [23] and
 38 the interaction between shear (or normal strain) flow and bubble volume
 39 change [24] form a tremendously complex flow field inside an injector noz-
 40 zle, where dynamic changes in the behaviour of vortices and vapour bubbles
 41 strongly affect the emerging fuel spray. Highly transient flow phenomena
 42 caused by the fast needle response times, give rise to formation of vortical
 43 structures and therefore, to string cavitation [25]. Transient effects have also
 44 been correlated to increased probability of surface erosion damage, which
 45 is attributed to both, geometric and string cavitation [26]. Cavitation in
 46 simplified nozzle replicas has been visualized even at pressures as high as
 47 2000bar, as shown in [27, 28]. Remarkably, in very recent studies, sonolu-

48 minescence from cavitation collapse observed in a simplified nozzle replica
 49 has been observed for the first time[29] and a neutron imaging technique has
 50 been developed overcoming the disadvantages of using materials transparent
 51 to visible light[30]. All aforementioned studies report data from one or just a
 52 few injection events. The group of the authors has reported in [31, 32, 33]] for
 53 the first time ensemble averaged images of cavitation developing in a real-size
 54 6-hole transparent tip nozzle for single and pilot-main split injections up to
 55 400bar. Data from these investigations are further reported here and utilized
 56 for validation of the newly developed models. Only the very recent work of
 57 [34] has extended the range of operating conditions (injection pressures up
 58 to 1000bar and back pressures up to 30bar) and geometrical features studied
 59 (hydro erosively ground inlet orifice) for long injections.

60 Given the limited information around the flow structure inside diesel
 61 injectors, fuel injection equipment manufacturers require robust predictive
 62 Computational Fluid Dynamics (CFD) tools, in order to understand the
 63 physical mechanisms taking place during injection. From a physical view-
 64 point, modelling of such flow conditions requires the fluid compressibility
 65 [35], mass transfer (cavitation, flash boiling, evaporation etc.) and heat
 66 transfer [36, 37, 38] to be taken into account, which increase the complexity
 67 as well as the computational cost of the simulations. Additionally, the fluid
 68 dynamic processes occur at high Reynolds number and therefore accounting
 69 for the effect of turbulence structures and vortex dynamics, is key in explain-
 70 ing how the spray is formed [39, 40, 41, 42]; this can only be resolved using

71 very fine computational grids and scale resolving simulations such as Large
72 Eddy Simulation (LES).

73 Recent LES including dynamic needle movement for the in-nozzle flow
74 includes the work of Battistoni et al. [43] who simulated the start and end
75 of injection for single hole nozzle using the cut cell cartesian method for
76 modelling the boundary movement and a homogeneous relaxation model for
77 cavitation phenomena. The work concludes that URANS predictions for the
78 residual liquid back flow occur without fragmentation, while in LES liquid
79 breaks up generating complex three dimensional structures. The URANS ap-
80 proach predicted at the end of the injection an annular void region stemming
81 from the needle seat, which then re-condenses as the pressure is recovered.
82 This was not observed in LES, where regions of low pressure are produced
83 even in areas detached from the needle seat. The predicted near spray region
84 was also different as no ligaments were formed in URANS; instead diffusion
85 disperses the liquid in the surrounding air even if integral values like sac
86 pressure and liquid volume fraction were not greatly affected. Ligament for-
87 mation and gas ingestion into the nozzle at the end of injection are predicted,
88 as observed experimentally in Phase Contrast X-ray images (for additional
89 Phase Contrast X-ray studies see for example [9, 44]). The start-of-injection
90 simulation shows how gas is ejected first, and liquid fuel starts being in-
91 jected with a delay. The main result of these analyses is that if the sac is
92 initially filled with gas, the liquid exit is delayed several tens of μs after the
93 start of needle movement, which is in good agreement with the experimen-

94 tal evidence. This delay is of the order of $100\mu s$, and it is compatible with
 95 the duration of the first slow rising part of the needle movement. Orley et
 96 al. [45] used the cut cell cartesian method to simulate with implicit LES, a
 97 barotropic homogeneous equilibrium model for cavitation and a fully com-
 98 pressible 3-phase flow model a complete 9-hole diesel injector. The focus of
 99 the work was on the vortical development of the flow and the assessment
 100 of erosion sensitive areas during the operation of the injector. After the in-
 101 jector closing, strong collapse events of vapor structures in the needle seat
 102 and the sac hole cause the formation of violent shock waves. The authors
 103 highlighted that a fully compressible description of the flow is essential to
 104 capture such phenomena. It was also concluded that despite steady needle
 105 simulations capturing the main flow features reasonably well, vapor creation
 106 during the closing phase of the needle valve requires information on the pre-
 107 viously developed flow; thus, reliable prediction of erosion-sensitive areas
 108 due to collapse events during and after the closing of the needle can only
 109 be predicted accurately by including the unsteady needle motion. Finally
 110 the work of Koukouvinis et al. [35] used a 2-phase dynamic needle approach
 111 based on a combination of layering and stretching algorithms together with
 112 a Rayleigh-Plesset based cavitation model with increased mass transfer, to
 113 compute the opening phase of two different injector designs; the findings
 114 have correlated the pressure peaks in the domain with areas that suffer from
 115 erosion. Whichever the chosen modelling approach may have been, previous
 116 studies have lacked validation [45], had indirect validation [35] or were not of

117 direct relevance to modern applications [43], since a single hole nozzle lacks
118 the complex sac recirculation flow present in modern diesel injectors.

119 The current work, to the best of the authors knowledge, presents for
120 the first time a successful 3-phase LES of a diesel pilot injection including
121 the compressibility of the phases, cavitation effects and the needle valve
122 movement of a real size 6 hole nozzle for which validation is performed against
123 transparent nozzle tip visualisations. The need to employ LES derives from
124 the need to predict the complex vortical flow and liquid structures inside the
125 sac during and after injection; moreover, and as it is shown, replicating the
126 observed phenomena requires the inclusion of compressibility effects.

127 The present paper is structured in the following way: first an overview
128 on the experimental results is given for a diesel pilot injection visualization
129 of a transparent nozzle tip. Then the numerical methodology employed is
130 described in detail, followed by the comparison of the CFD results with the
131 transparent nozzle visualisations for which good agreement is obtained and
132 interpretation of the observed phenomena is provided.

133 **2. Experimentally observed multiphase phenomena**

134 The development of the 3-phase simulation methodology has been vali-
135 dated against high speed visualisations of a transparent Delphi Technologies
136 Diesel 6-hole nozzle tip manufactured by City, University of London. The
137 metallic injector nozzle tip was substituted with a transparent acrylic tip.
138 The design is a standard serial production geometry, i.e not just a multi-hole

139 nozzle, but a fully operational, serial production type. The detailed results
 140 and findings of that experimental campaign as well as the setup details were
 141 reported in [31, 32, 33] and will not be repeated here. The 6-hole transparent
 142 tip has holes with no taper (zero conicity) and a nominal diameter (D) of
 143 $160\mu m$. The electrical pulse activation width for a pilot injection was $0.5ms$.
 144 High speed cameras recorded the events at a frame rate of $30000fps$. An
 145 example of a pilot injection for a rail pressure of 300bar into atmospheric
 146 conditions can be found in Figure 1. Given the image acquisition rate, the
 147 pilot injection including all major events after closing lasts for 24 frames.
 148 As discussed in [32, 33] air trapped in the sac after the end of the injection
 149 aggregates forming bubbles in the sac and occupying part of the hole. Prior
 150 to $233.33\mu s$ after the electrical trigger, no change is observed and therefore
 151 images are not shown. Then the trapped bubble shows slight expansion due
 152 to the initial volume created by the needle as it starts lifting ($300\mu s$ after
 153 the trigger) and subsequent compression ($400\mu s$ after the trigger) highlight-
 154 ing the need to model air compressibility. This is followed by void coming
 155 from the seat passage and its advection into the hole ($500\mu s$ after the trigger).
 156 Then, due to flow acceleration at the hole entrance, void structures are seen in
 157 the hole during the opening phase ($600\mu s$ after the trigger). During the nee-
 158 dle closing phase, vapour increases substantially in the hole and void coming
 159 from the seat reappears ($633.33\mu s$ after trigger). At the end of the injection,
 160 the sac gets full with bubbles and the spray greatly weakens ($733.33\mu s$ after
 161 the trigger), followed by what seems to be air suction ($766.66\mu s$ after the

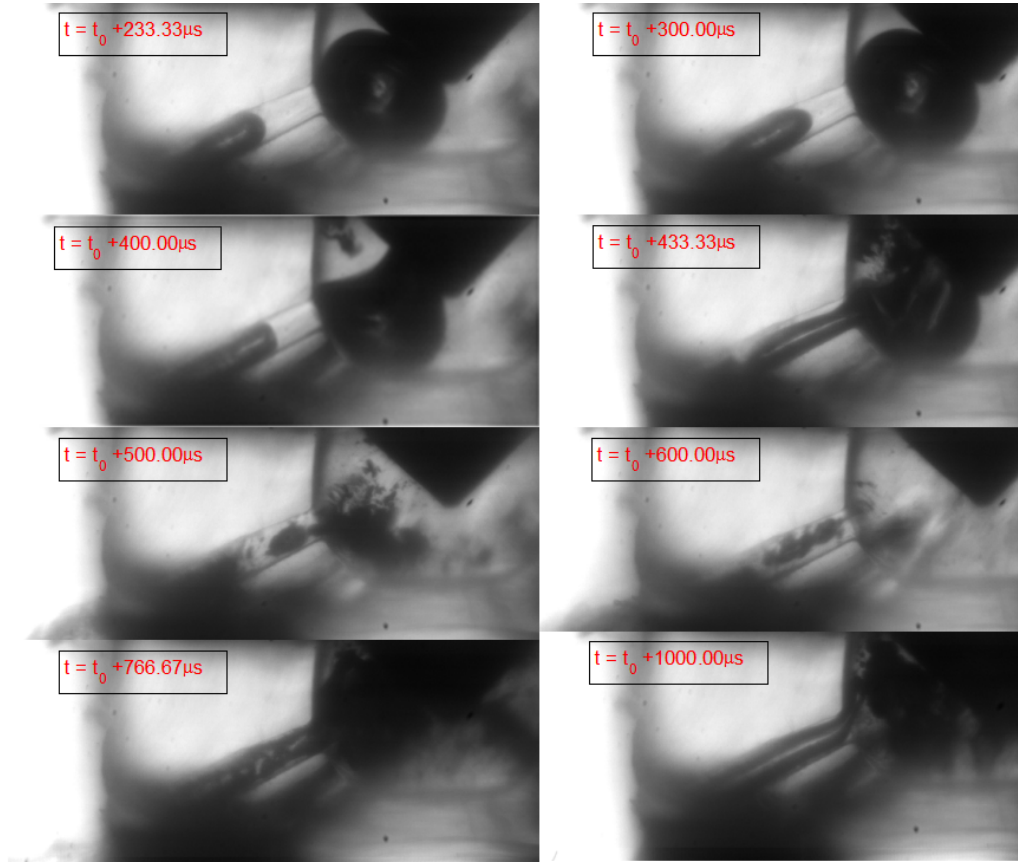


Figure 1: Experimental results. Time sequence of a pilot injection transparent nozzle tip visualisation.

162 trigger). Finally, a bubbly mixture is observed floating in the sac as well as
 163 an oscillatory movement of the air in the hole ($1000\mu s$ after the trigger). An
 164 important input for nozzle flow moving needle simulations is the needle lift
 165 profile which was extracted from the images [31, 32, 33].

166 3. Modelling approach

167 The simulations are computed using the commercial CFD code ANSYS
 168 Fluent [46]. The nozzle flow is solved using a homogeneous, three-phase
 169 mixture model (liquid fuel, vapour fuel and air) where all phases share same
 170 velocity, pressure and temperature. The code is supplemented with user
 171 defined functions (UDFs) for implementation of the thermo-hydraulic prop-
 172 erties of diesel and the needle movement.

173 3.1. Multiphase model

174 The properties appearing in the transport equations are determined by
 175 the presence of the component phases in each control volume. Defining α_{liq} ,
 176 α_{vap} , α_{air} as the volume fraction of liquid fuel, air and vapour fuel in a cell,
 177 respectively, the density in each cell is given by: $\rho = \alpha_{liq}\rho_{liq} + \alpha_{vap}\rho_{vap} +$
 178 $\alpha_{air}\rho_{air}$.

179 All other properties (e.g. viscosity) are computed in this manner. Ob-
 180 viously, the volume constraint $\alpha_{liq} + \alpha_{air} + \alpha_{vap} = 1$, in each cell must be
 181 respected. The solved equations consist of the continuity, momentum and
 182 energy of the mixture, and the mass conservation equations for the vapor
 183 and the air:

$$\frac{\partial \rho}{\partial t} + \nabla \cdot (\rho \mathbf{v}) = 0 \quad (1)$$

$$\frac{\partial \rho \mathbf{v}}{\partial t} + \nabla \cdot (\rho \mathbf{v} \mathbf{v}) = -\nabla p + \nabla \cdot \sigma \quad (2)$$

$$\frac{\partial \rho E}{\partial t} + \nabla \cdot (\mathbf{v}(\rho E + p)) = \nabla \cdot (k_{eff} \nabla T) + \sigma \cdot \mathbf{v} \quad (3)$$

$$\frac{\partial \alpha_{vap} \rho_{vap}}{\partial t} + \nabla \cdot (\alpha_{vap} \rho_{vap} \mathbf{v}) = R_e - R_c \quad (4)$$

$$\frac{\partial \alpha_{air} \rho_{air}}{\partial t} + \nabla \cdot (\alpha_{air} \rho_{air} \mathbf{v}) = 0 \quad (5)$$

184 The source terms R_e and R_c represent the mass transfer between liquid
 185 and vapour phase due to cavitation. The effective viscous stress tensor is
 186 defined as $\sigma = \tau + \tau_t = \mu(\nabla \mathbf{v} + (\nabla \mathbf{v})^T) + \tau_t$,

187 where μ is the viscosity of the mixture and τ_t are the turbulent stresses
 188 defined per the turbulence model being used. The energy is computed as the
 189 mass average for each phase and the internal energy of each phase is based
 190 on the local thermodynamic conditions of that phase [37].

191 The source terms appearing in the vapour volume fraction transport equa-
 192 tion ($R_e - R_c$) represent the mass transfer between fuel liquid and vapour
 193 phases due to cavitation bubble expansion and collapse respectively. The
 194 calculation of these values is based on the Rayleigh-Plesset equation describ-
 195 ing bubble expansion and collapse [47], and its magnitude is based on the
 196 Zwart-Gerber-Belamri cavitation model [48] which reads as:

$$R_e = F_{vap} \frac{(3\alpha_{nuc}(1 - \alpha_{vap})\rho_{vap})}{R_b} \sqrt{\frac{2 \max((p_{vap} - p), 0)}{3 \rho_{liq}}} \quad (6)$$

$$R_c = F_{cond} \frac{(3\alpha_{vap}\rho_{vap})}{R_b} \sqrt{\frac{2}{3} \frac{\max((p - p_{vap}), 0)}{\rho_{liq}}} \quad (7)$$

197 F_{vap} and F_{cond} are empirical calibration coefficients, α_{nuc} is the volume
 198 fraction associated with the nuclei contained in the liquid and R_b the assumed
 199 bubble radius and p_{vap} is the vapour pressure. According to [48], values of
 200 $R_b = 10^{-6}m$, $\alpha_{nuc} = 5 \times 10^{-4}$, $F_{vap} = 50$, $F_{cond} = 0.01$ give reasonable re-
 201 sults in a wide range of flows. Nevertheless, as discussed in [49] the mass
 202 transfer magnitude for these values could be insufficient creating areas of
 203 unrealistic liquid tension and not reproducing correctly the Rayleigh-Plesset
 204 bubble collapse, the suggested solution is to increase the empirical calibra-
 205 tion coefficients several orders of magnitude to approximate the model to
 206 a Homogeneous Equilibrium Model (HEM). However, within this work the
 207 original coefficients published in [48] were used.

208 3.2. Turbulence model

209 The target when using LES is to capture the large scales that are depen-
 210 dent of the physical domain simulated while modelling the sub-grid turbulent
 211 scales. This is achieved by filtering of the Navier-Stokes equations using a
 212 spatial low-pass filter determined by the cell size of the computational domain
 213 used. This operation leaves the flow equations unchanged, but transforms
 214 the equations into equations for the filtered magnitudes [50]. During this
 215 operation terms in the equations appear representing the sub grid scale con-
 216 tributions to the equations of motions and have to be modelled. The closure

217 of the model requires calculating a suitable sub grid turbulent dissipation
 218 (viscosity) μ_t . For such purpose, the Wall-Adapting Local Eddy-Viscosity
 219 (WALE) model is chosen [51]. This model is capable of correctly reproduc-
 220 ing the correct turbulence wall behaviour ($\mu_t \sim o(y^3)$) and becomes 0 at
 221 $y = 0$, being y the normal distance to the wall. Another advantage is that
 222 it returns a zero turbulent viscosity for laminar shear flows which allows
 223 the correct treatment of laminar zones in the domain, this is necessary for
 224 modelling the start of injection when flow velocities are low.

225 3.3. *Fluid properties*

226 High injection pressures and low lifts cause high injection speed velocities
 227 and important transient heating effects making an incompressible approach
 228 unjustifiable [36, 37, 35]. Even if for the transparent nozzle tip testing con-
 229 ditions the pressure is lower than engine conditions, the diesel liquid phase
 230 is modelled as a compressible liquid based on the measurements made for
 231 the calibration oil Normafluid ISO4113. This is the usual fuel for testing
 232 and calibrating diesel fuel injection systems in laboratory at an industrial
 233 level. All diesel properties that follow are taken from [52, 53], where de-
 234 tails on how the measurement methodology, range of validity, method for
 235 fitting the coefficients and their values can be found. (see Figure 2 for plots
 236 of the density and viscosity values for different pressures and temperatures)
 237 These properties were implemented into ANSYS Fluent following the avail-
 238 able User-Defined-Real-Gas-Model (UDRGM) functionality as in [37]. As

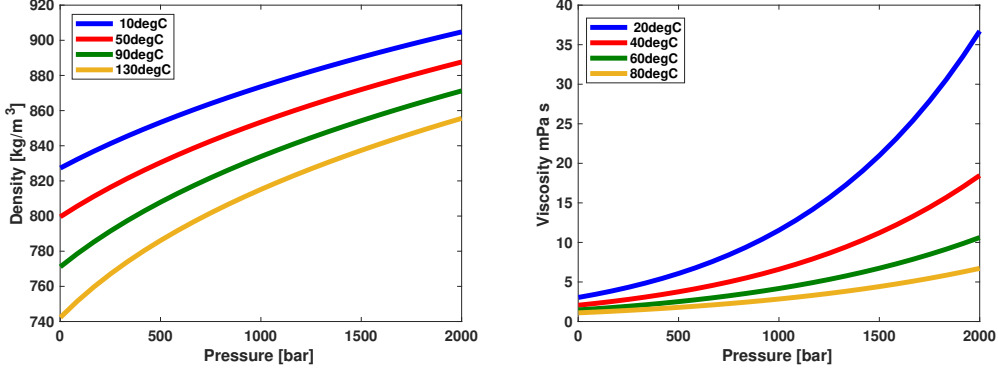


Figure 2: Diesel fuel properties implemented. Density (left) and viscosity (right) diesel fuel properties used.

mentioned in the experimental results section, air compressibility effects are observed during the sac filling event and therefore the air density is modelled as an ideal gas with equation of state $p = \rho RT$.

3.4. Moving mesh methodology. Mesh generation and boundary conditions.

Modelling the dynamic movement of the needle is inherently difficult. At low lifts the cells in the seat are squeezed into very small gaps deteriorating their quality, which can have an impact on the robustness and accuracy of the simulation. Moreover, the contact between walls is not trivial to model since the continuity of the mesh is broken. Recent advances have been reported in [54] where the immersed boundary method has allowed simulations to be performed even at zero needle lift; however, this method has not been adopted here and as a compromise, the closed needle is modelled using the seat surface as a wall when the needle lift is below $1\mu m$.

The approach followed is based on an interpolation approach between two

253 topologically identical meshes (key-grids) with the same number of cells and
 254 was already employed by the authors in [55]. The initial mesh has a $1\mu m$
 255 lift and the high lift mesh is based on the maximum lift reached for the pilot
 256 injection $36\mu m$. Based on the node position of this two meshes any interme-
 257 diate lift is achieved by linear interpolation between the node position of the
 258 two key-grids. Another difficulty associated is the loss of resolution in the
 259 seat passage as the needle reaches high lifts, this requires interpolating the
 260 results into another pair of key-grids such as in [37]. For the pilot injection
 261 cases considered here, this was not needed due to the relatively low lift at-
 262 tained ($36\mu m$). Moreover, in order to save computational resources, just a
 263 60° sector is model (one hole) based on the nominal (target) geometry. Figure
 264 3 (left) shows the computational domain, consisting of different surfaces; the
 265 hole, housing, needle, seat inlet and side surfaces. Additionally, a 2mm long
 266 conical discharge volume is added in order to move away the outlet boundary
 267 condition from the areas of interest. The computational mesh used for the
 268 LES flow simulation is a fully hexahedral mesh.

269 The LES settings are adapted from the basis of the previous successful
 270 studies on diesel [39, 40, 41, 42] and gasoline [55, 56] direct injection and
 271 primary breakup simulations. In order to choose the appropriate filter/mesh
 272 size for the LES, the Taylor micro-scales (λ_g) have been estimated. This
 273 length scale is the intermediate length scale at which fluid viscosity signif-
 274 icantly affects the dynamics of turbulent eddies in the flow [57]. For the
 275 flow inside the transparent tip, the Reynolds number based on the nozzle

276 hole diameter, outlet pressure and inlet temperature can be estimated to be
 277 $Re = \frac{(\rho V D)}{\mu} \sim 13000$. The Taylor micro-scales can then be approximated by
 278 [50]: $\lambda_g = \sqrt{\frac{10D}{Re}} = 4.4\mu m$. However, in order to resolve the smallest eddies
 279 close to the wall, the non-dimensional wall distance based on the friction
 280 velocity has to be of the order of 1 ($y^+ \sim 1$) [50]. Therefore, additional
 281 refinement close to the walls is needed. An estimate of this value based on
 282 the turbulent boundary layer theory yields a cell wall distance of $\sim 0.2\mu m$.
 283 In order to reach a value of $\sim 5\mu m$ in the bulk flow without increasing in
 284 excess the number of cells, a cell growth ratio of 1.1 was applied in the wall.
 285 Under these constraints, a $\sim 5M$ element mesh was produced, with a vol-
 286 ume change between neighbouring cells below 3, minimum cell angle of 27°
 287 and $3D$ determinant (normalized triple product of the vectors starting from
 288 each cell node) above 0.6 for both key-grids. Special care was taken to re-
 289 fine the needle seat area in the stream-wise direction in order not to exceed
 290 for low lifts aspect ratios of 100 in the direction of the bulk flow. Figure 3
 291 (right) depicts the two meshes needed for the interpolation method, and a
 292 front view of the mesh showing the additional refinement in the seat area.
 293 A pressure boundary conditions was applied to the inlet of the domain. The
 294 pressure at the injector entrance in the high-pressure pipe was taken from
 295 the experimentally recorded values for every individual injection event. Dur-
 296 ing the opening phase, pressure decreases at the injector entrance due to the
 297 increasing flow through it. At the end of the injection an over pressure is
 298 observed due to the water hammer effect after needle closing. The pressure

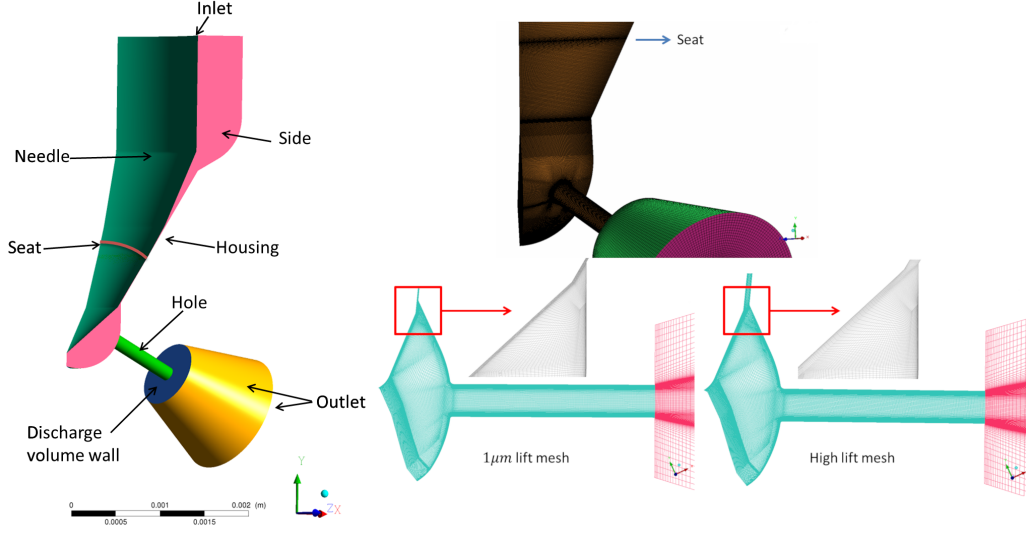


Figure 3: Geometrical model and mesh. Domain simulated and boundary conditions (left). Mesh showing seat refinement (right-top) and mesh cross section for both high and low lift meshes (right-bottom).

299 at the entrance of the injector was provided in [31]. A temperature of $300K$
 300 was chosen for the flow entering the domain and an air mass fraction value
 301 of 2×10^{-5} was imposed to take into account the possible dissolved air since
 302 it is a typical value for fuel or water exposed to ambient pressure [58]. The
 303 non-slip boundary conditions was applied to the non-moving wall (housing,
 304 hole, discharge volume wall, and, seat surface below $0.1\mu m$) as well as to the
 305 needle according to the motion profile resulting from the needle lift profile
 306 extracted from the images [31]. Periodic boundary condition have been ap-
 307 plied to the side surfaces. And fixed pressure outlet was applied to the outlet
 308 surfaces, with pressure 1bar and $300K$ and air volume fraction prescribed as
 309 1 in the case of back-flow.

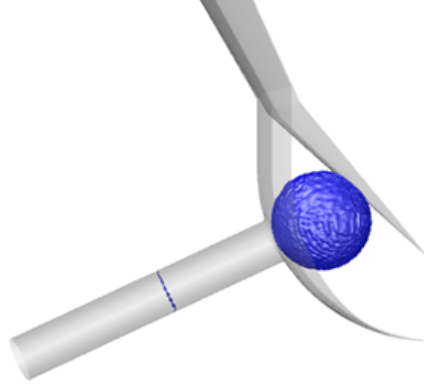


Figure 4: Initial simulation instant. Iso-surface of 0.5 liquid volume fraction and a mid-plane for the initial instant.

310 The experimental images of the transparent nozzle show trapped air bub-
 311 bles inside the injector before the start of injection. The mechanism behind
 312 the appearance of this bubble is not straight forward to derive from the ex-
 313 perimental images. Regardless, the LES nozzle flow simulation is initialised
 314 in qualitatively similar way; half of the hole is filled with air and an air
 315 spherical bubble is included in the sac (see Figure 4).

316 The computational domain above the seat surface is initialised at the
 317 pressure corresponding to that instant. Below the seat, the simulation is
 318 initialised at a pressure of $1bar$. All the domain is initialised at a temperature
 319 of $300K$ and with zero velocity. For the closing phase the movement of
 320 the needle is stopped when it reaches $1\mu m$ however the seat surface is not
 321 switched from interior to wall until the needle lift profile reaches $0.1\mu m$.

322 The solver used is segregated and pressure-based. The pressure-velocity
 323 coupling is achieved using the SIMPLEC algorithm [59]. The continuity

324 equation was discretised using a second order upwind scheme [60] while for
 325 the momentum equation a bounded central differencing scheme based on the
 326 normalized variable diagram (NVD) approach together with the convection
 327 boundedness criterion (CBC) [61] was used. The bounded central differenc-
 328 ing scheme is a composite NVD-scheme that consists of a pure central dif-
 329 ferencing, a blended scheme of the central differencing and the second-order
 330 upwind scheme, and the first-order upwind scheme. The first-order scheme is
 331 used only when the CBC is violated. This scheme has small numerical dissi-
 332 pation and sufficient numerical stability for industrial LES simulations [62].
 333 Discretisation of the volume fraction equations was done with the quadratic
 334 upstream interpolation for convective kinetics (QUICK) scheme (in order to
 335 capture the high density ratios) [60], pressure interpolation with the body
 336 force weighted scheme [46] and the temperature equation was discretised with
 337 a first order upwind scheme. Finally the calculation of gradients was done
 338 using the Least Squares Cell-Based method.

339 The used solver is pressure-based and therefore the simulation stability
 340 is not limited by the acoustic wave propagation time scale. However, tem-
 341 poral resolution for LES requires minimum diffusion for the advection of the
 342 turbulent eddies. Therefore, an adaptive time step method is employed to en-
 343 sure the advection CFL number stays below 1 throughout the computational
 344 domain.

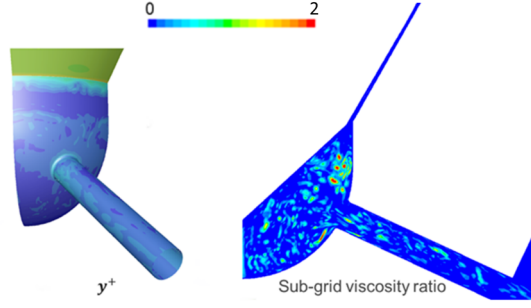


Figure 5: Mesh resolution evaluation. y^+ contours on the nozzle wall (left) and sub-grid viscosity ratio (right) for highest needle lift during the pilot injection.

3.5. *LES mesh quality evaluation*

The instantaneous fields of sub-grid viscosity ratio and y^+ for a characteristic moment at the highest lift ($t = 0.608ms$) are shown in Figure 5. Based on the y^+ the boundary layer resolution can be assessed; this value only exceeded 1 in areas above the seat and gradually transitions to values well under 1 ensuring a good wall shear resolution for the small eddies near the walls. Spatial resolution can be evaluated from the sub-grid viscosity ratio, which is defined as the sub-grid scale viscosity introduced by the WALE model divided by the molecular viscosity. Its value is mostly under 1 throughout the domain peaking at values of around 2 in the separation region that occurs at the entrance of the sac due, confirming the suitability of the mesh.

4. Results and discussion

The evolution of the volume fraction inside the nozzle for the different phases is shown in Figure 6. Additionally, the imposed needle lift extracted

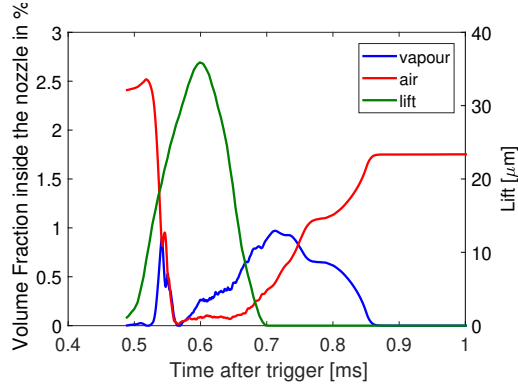


Figure 6: Integral results. Volume of vapour and air inside the nozzle and needle lift against time.

360 from the image sequence shown in Figure 1 is shown as well. The simulation
 361 is started at the physical time $0.4874ms$ coincident with a lift of $1\mu m$ for
 362 the imposed profile. During the opening phase it follows from this plot that
 363 initially there is air present inside the nozzle. This air is evacuated out of
 364 the nozzle while cavitation is generated showing a peak between $0.5ms$ and
 365 $0.6ms$ and decreases. As the injection transitions towards the closing phase
 366 the amount of vapour increases, showing a peak just after the needle closes,
 367 while the amount of air continually increases by a process of air suction as it
 368 will be shown in the following section.

369 A comparison between the transparent nozzle tip images and the simula-
 370 tion results at the start of the injection is shown in Figure 7. In particular,
 371 a snapshot of the predicted liquid volume iso-surface of 50 at $t = 0.532ms$
 372 is shown. At the early stages of the injection the simulation reproduces the
 373 compression of the air bubble inside the sac volume. The compression is
 374 caused by the pressure build up in the sac, showing the need for modelling

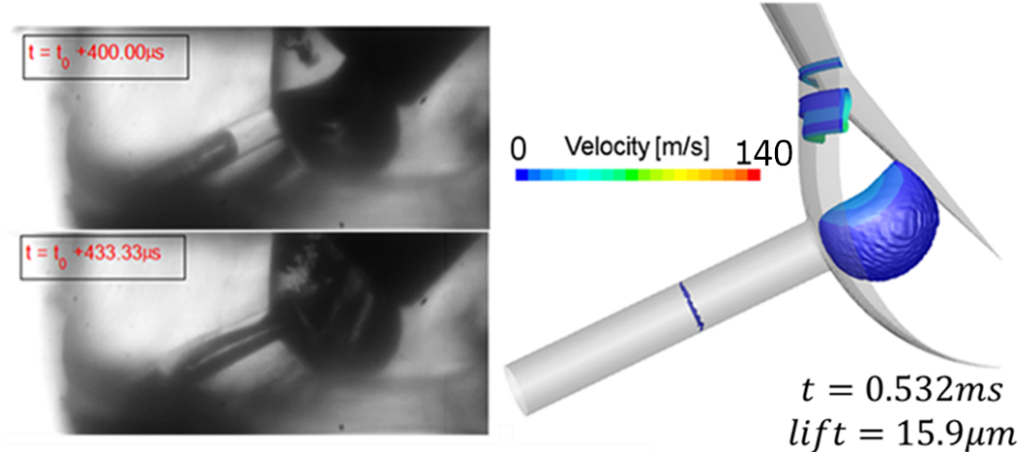


Figure 7: Start of injection results. Experimental visualisations (left), 50% liquid volume fraction iso-surface coloured by velocity magnitude (right).

the compressibility of the air. This is quickly followed by cavitation coming at the needle seat passage, due to flow separation and shear in this area.

Sample simulation results and the transparent nozzle tip images for the needle opening phase are shown in Figure 8. The CFD results indicate that cavitation produced at the sac entrance is transported directly into the hole. Simultaneously, the air bubble is further compressed and is pushed to recirculate parallel to the needle in the direction of the needle motion. Similarly to the experimental images, the air bubble is seen breaking down and mixing with any remaining cavitation into a fine bubbly mixture which is then advected into the hole.

As the needle lift increases and the flow further develops, the simulation indicates that air disappears from the sac volume, as seen in Figure 9. This is attributed to a combination of two effects. Firstly, the sac pressure build

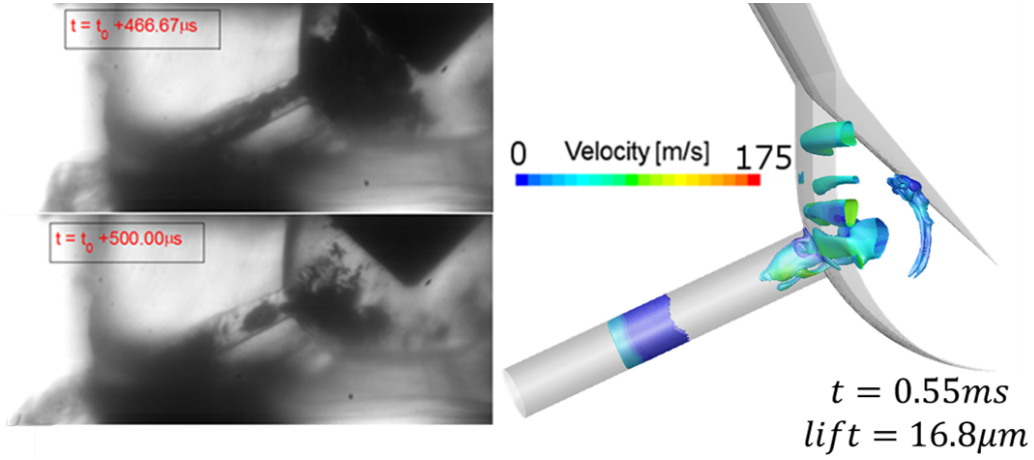


Figure 8: Needle opening phase results. Experimental visualisations (left), 50% liquid volume fraction iso-surface coloured by velocity magnitude (right).

up causes the air to be compressed, reducing its volume fraction. Secondly, as the air is trapped within the recirculation zone developing inside the sac volume, it enters into the injection hole, where it expands due to the local pressure drop at its entrance. This contributes to the void areas observed and suggests that the void observed experimentally is a combination of air and fuel vapour. In addition, part of the void visible in the simulation can be attributed to geometrical cavitation developed at the hole inlet upper lip which can also be seen from the experimental images.

The only two experimental frames available for the needle closing phase together with the simulation results are shown in Figure 10 (top). As the needle valve moves into the closing phase, the amount of void in the hole increases. This is in agreement with the simulation results from Figure 6, where volume content as a percentage of the injector volume of both air

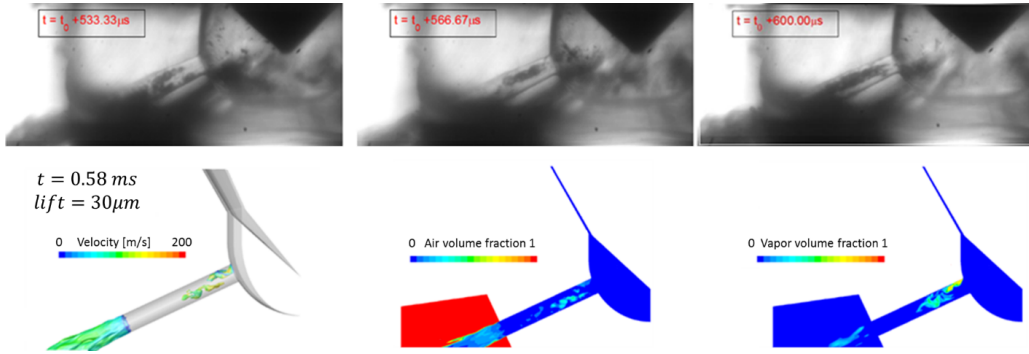


Figure 9: Results as flow further develops during the opening phase. Experimental visualisations for three time instances (top), 50% liquid volume fraction iso-surface coloured by velocity magnitude (bottom-left), air volume fraction contours (bottom-centre) and vapour volume fraction contours (bottom-right).

and vapour are plotted against time, it follows that these quantities increase during the needle closing phase. This void in the simulation has two sources, one from the unstable vortical flow from the sac coming into the hole and another due to geometrical cavitation in the hole inlet corner. Regarding the experimental results at very low lifts ($lift = 6\mu m$), a bubbly mixture appears in the sac and bubbles of size of the order of the hole diameter appear in the hole. At very low lifts ($lift = 6\mu m$), the simulation model predicts high velocities in the hole; however, since the flow coming from the seat is throttled, pressure loss in the sac is occurring and a void structure appears in front of the hole. The bubbly mixture in the sac volume correlates to the void structure created in front of the hole, which is predicted to be composed of a mixture of fuel vapour and expanded air. On the other hand, the visualised bubbles inside the hole correlate to the big amount of cavitation computed in the hole.

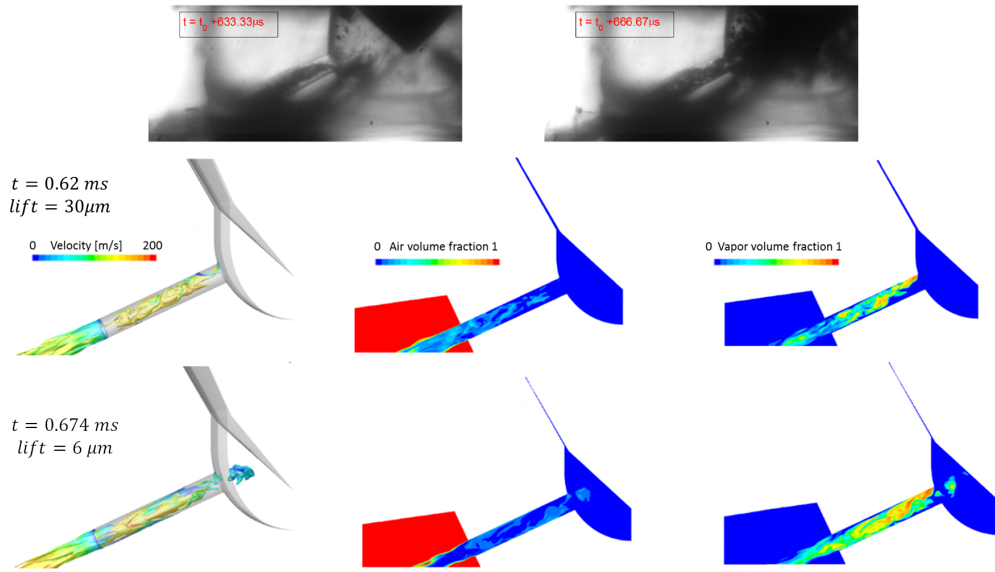


Figure 10: Needle closing results. Experimental visualisations for two time instants (top). Simulation results (center and bottom). For the simulation results 50% liquid volume fraction iso-surface coloured by velocity magnitude (left), air volume fraction contours (center) and vapour volume fraction contours (right) are presented.

415 A time sequence of the pressure field is presented in Figure 11. Before the
 416 needle valve closes, the predicted sac pressure is still higher than the ambient
 417 pressure ($t = 0.674ms$), but immediately after the needle valve closing ($t =$
 418 $0.698ms$) a pressure wave is generated that travels towards the sac volume;
 419 this leaves the sac pressure below the ambient pressure ($t = 0.77ms$). In
 420 agreement with Figure 6, where air volume fraction inside the nozzle is seen
 421 to increase after needle closing, this induces the spray to weaken and air to
 422 be sucked back from the ambient into the nozzle until the sac pressure is
 423 balanced with the exterior pressure ($t = 1ms$).

424 Evidence is also provided in Figure 12, which shows a time sequence
 425 of air and vapour volume fraction fields. It clearly depicts the weakening
 426 flow momentum in the injection hole ($t = 0.698ms$) leading to air suction
 427 ($t = 77ms$). Finally, due to the pressure balancing with the ambient pressure,
 428 vapour completely disappears ($t = 1ms$), indicating that shortly after the
 429 needle closing only liquid and air remain inside the sac volume.

430 5. Conclusions

431 This paper presents an investigation of cavitation and air interaction dur-
 432 ing a diesel pilot injection of a standard serial production six-hole geometry.
 433 The focus was to understand the complex interaction between the needle mo-
 434 tion, cavitation formation and development, and gas suction. The strategy
 435 followed has been to use high speed visualisations of a transparent nozzle tip
 436 to record the multiphase phenomena and to use CFD to explain the physics

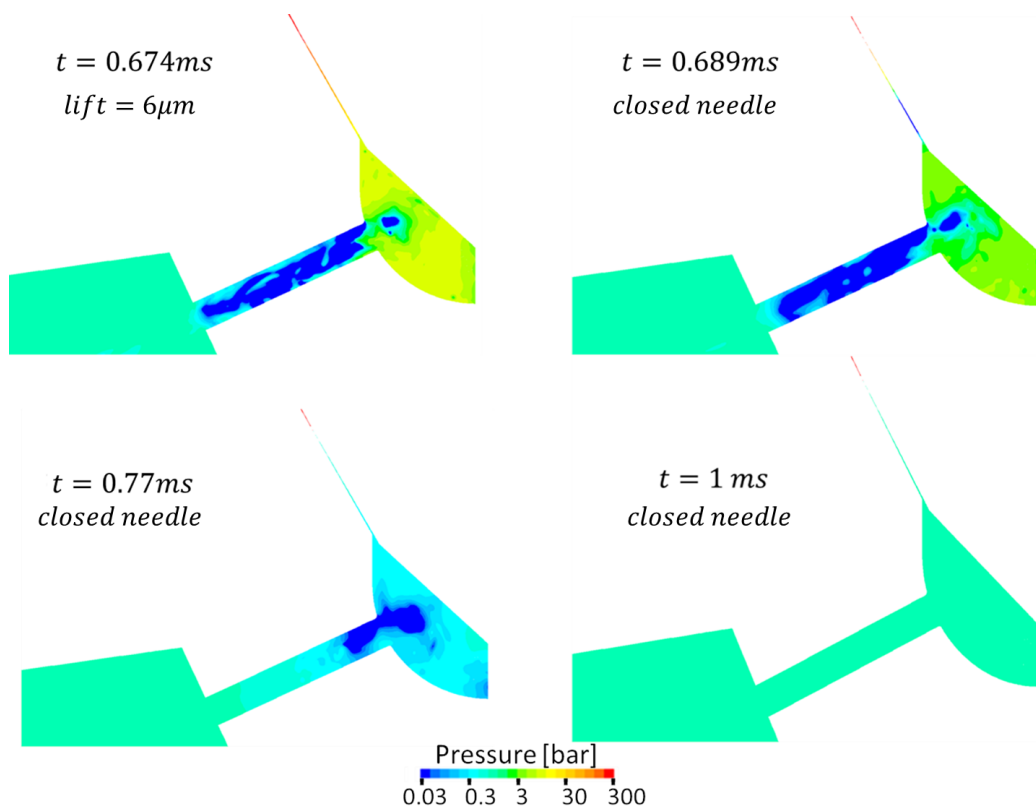


Figure 11: Pressure field time sequence. Notice that logarithmic scale has been used.

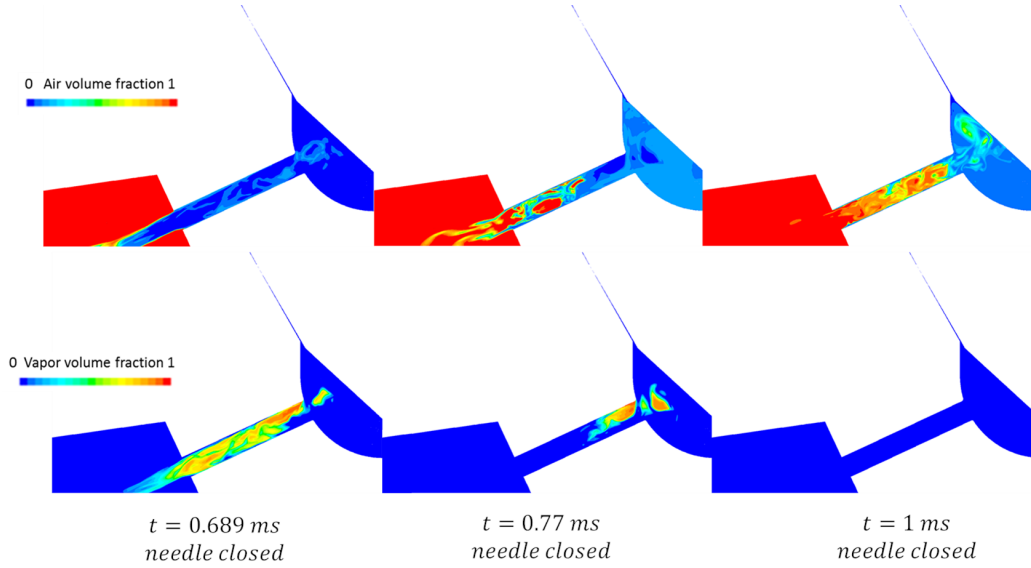


Figure 12: After needle closing results. Time sequence for air (top) and vapour (bottom) volume fraction fields.

437 behind the observations. The CFD methodology includes LES turbulence
 438 modelling, the needle valve boundary movement, cavitation effects through
 439 a Rayleigh-Plesset based cavitation model, and the compressibility of air
 440 and fuel. Starting from a flow field initialised according to the experimental
 441 observations (with an air bubble in the sac and a big portion of the hole
 442 filled with air), the main flow features observed are replicated by the simu-
 443 lations. In particular the following phenomena experimentally noticed have
 444 been explained and reproduced:

- 445 • The compression of the initial air bubble due to sac pressure build
 446 up. The inclusion of air compressibility in the simulation can be very
 447 relevant even for modest injection pressures in order to replicate the
 448 air compression in the sac at the start of the injection as well as the

449 air expansion in the injection hole and sac.

450 • The appearance of cavitation stemming from the sac entry at the start
451 of the injection, due to flow separation and shear.

452 • The sac flow recirculation in the sac and flow patterns inside the hole.
453 One part of the void observed in the simulation can be attributed to
454 cavitation both geometrical (developed at the hole inlet upper lip) and
455 vortical (due to complex flow structure coming from the sac). Further-
456 more, the initial air inside the nozzle expands in the hole contributing
457 to the void areas observed. This shows that the void observed experi-
458 mentally is a combination of both air and fuel vapour.

459 • An increase of void inside the hole and in the sac during the needle
460 valve closing. The underlying reason being the flow throttling, since
461 liquid momentum is still high but flow passage very restricted.

462 • The air suction after the needle closing. The closure of the valve creates
463 an expansion wave that leaves the sac pressure below the ambient. This
464 induces vapour creation and air expansion in the sac and consequently
465 air is sucked from the ambient into the nozzle. When the pressure in
466 the sac is recovered, all vapour collapses. Therefore it is shown that
467 the remaining foam at the end of the injection consists of a liquid and
468 air mixture.

469 Acknowledgements

470 The European Union Horizon-2020 Research and Innovation Program
471 funding to Eduardo Gomez Santos (No 675676), the ANSYS HPC research
472 license grant to Delphi Technologies, and the CPU time granted by Gcompute
473 are highly appreciated.

474 References

- 475 [1] European-Comission, “Commission regulation (eu) 2017/1151 of 1 june
476 2017,” July 2017. [https://eur-lex.europa.eu/legal-content/EN/
477 TXT/?uri=CELEX:02017R1151-20190101](https://eur-lex.europa.eu/legal-content/EN/TXT/?uri=CELEX:02017R1151-20190101).
- 478 [2] S. Shundoh, M. Komori, K. Tsujimura, and S. Kobayashi, “Nox re-
479 duction from diesel combustion using pilot injection with high pres-
480 sure fuel injection,” in *SAE Technical Paper*, SAE International, 1992.
481 <https://doi.org/10.4271/920461>.
- 482 [3] D. A. Pierpont, D. T. Montgomery, and R. D. Reitz, “Reducing par-
483 ticulate and nox using multiple injections and egr in a d.i. diesel,” in
484 *SAE Technical Paper*, SAE International, 1995. [https://doi.org/10.
485 4271/950217](https://doi.org/10.4271/950217).
- 486 [4] H. Afzal, C. Arcoumanis, M. Gavaises, and N. Kampanis, “Internal flow
487 in diesel injector nozzles modelling and experiments,” in *Fuel injection
488 systems. Proceedings*, 1999. [https://doi.org/10.1016/j.fuel.2013.
489 08.060](https://doi.org/10.1016/j.fuel.2013.08.060).

- 490 [5] E. Giannadakis, M. Gavaises, and C. Arcoumanis, “Modelling of cavi-
491 tation in diesel injector nozzles,” *Journal of Fluid Mechanics*, vol. 616,
492 pp. 153–193, 2008. <https://doi.org/10.1017/S0022112008003777>.
- 493 [6] I. H. Sezal, S. J. Schmidt, G. H. Schnerr, M. Thalhamer, and M. Förster,
494 “Shock and wave dynamics in cavitating compressible liquid flows in
495 injection nozzles,” *Shock Waves*, vol. 19, pp. 49–58, Apr 2009. <https://doi.org/10.1007/s00193-008-0185-3>.
- 497 [7] F. Salvador, J.-V. Romero, M.-D. Rosello, and J. Martinez-Lopez, “Val-
498 idation of a code for modeling cavitation phenomena in diesel injector
499 nozzles,” *Mathematical and Computer Modelling*, vol. 52, no. 7, pp. 1123
500 – 1132, 2010. <https://doi.org/10.1016/j.mcm.2010.02.027>.
- 501 [8] M. Ikemoto, K. Shimode, K. Omae, and N. Toda, “Diesel spray and com-
502 bustion development using nozzle flow visualization , spray and combus-
503 tion analyses,” in *Proceedings of International Congress : SIA Power-*
504 *train -Rouen*, 2016.
- 505 [9] S. Moon, W. Huang, Z. Li, and J. Wang, “End-of-injection fuel dribble of
506 multi-hole diesel injector: Comprehensive investigation of phenomenon
507 and discussion on control strategy,” *Applied Energy*, vol. 179, pp. 7 – 16,
508 2016. <https://doi.org/10.1016/j.apenergy.2016.06.116>.
- 509 [10] H. Kyu Suh and C. Sik Lee, “Effect of cavitation in nozzle orifice on the
510 diesel fuel atomization characteristics,” *International Journal of Heat*

511 *and Fluid Flow*, vol. 29, pp. 1001–1009, 08 2008. [https://doi.org/10.](https://doi.org/10.1016/j.ijheatfluidflow.2008.03.014)
512 [1016/j.ijheatfluidflow.2008.03.014](https://doi.org/10.1016/j.ijheatfluidflow.2008.03.014).

513 [11] R. Miranda, H. Chaves, U. Martin, and F. Obermeier, “Cavitation
514 in a transparent real size vco injection nozzle,” in *Proceedings of the*
515 *9th International conference on liquid atomisation and spray systems,*
516 *ICLASS, Sorrento*, 2003.

517 [12] I. Gilles-Birth, M. Rechs, U. Spicher, and S. Bernhardt, “Experimen-
518 tal investigation of the in-nozzle flow of valve covered orifice nozzles for
519 gasoline direct injection,” in *Proceedings of the 7th International sym-*
520 *posium on internal combustion diagnostics, Baden-Baden*, 2006.

521 [13] C. Arcoumanis, H. Flora, M. Gavaises, and M. Badami, “Cavitation
522 in real-size multi-hole diesel injector nozzles,” in *SAE 2000 World*
523 *Congress*, SAE International, mar 2000. [https://doi.org/10.4271/](https://doi.org/10.4271/2000-01-1249)
524 [2000-01-1249](https://doi.org/10.4271/2000-01-1249).

525 [14] C. Arcoumanis, M. Gavaises, H. Flora, and H. Roth, “Visualisation of
526 cavitation in diesel engine injectors,” *Mecanique & Industries*, vol. 2,
527 no. 5, pp. 375 – 381, 2001. [http://www.sciencedirect.com/science/](http://www.sciencedirect.com/science/article/pii/S1296213901011198)
528 [article/pii/S1296213901011198](http://www.sciencedirect.com/science/article/pii/S1296213901011198).

529 [15] H. Roth, E. Giannadakis, M. Gavaises, C. Arcoumanis, K. Omae,
530 I. Sakata, M. Nakamura, and H. Yanagihara, “Effect of multi-injection
531 strategy on cavitation development in diesel injector nozzle holes,” in

- 532 *SAE 2005 World Congress & Exhibition*, SAE International, apr 2005.
533 <https://doi.org/10.4271/2005-01-1237>.
- 534 [16] C. Arcoumanis, M. Gavaises, E. Abdul-Wahab, and V. Moser, “Mod-
535 eling of advanced high-pressure fuel injection systems for passenger car
536 diesel engines,” in *International Congress & Exposition*, SAE Interna-
537 tional, mar 1999. <https://doi.org/10.4271/1999-01-0910>.
- 538 [17] N. Mitroglou and M. Gavaises, “Cavitation inside real-size fully trans-
539 parent fuel injector nozzles and its effect on near-nozzle spray forma-
540 tion,” in *DIPSI workshop on droplet impact phenomena and spray in-*
541 *vestigations, University of Bergamo, Italy*, 2011.
- 542 [18] H. Chaves, R. Miranda, and R. Knake, “Particle image velocimetry mea-
543 surements of the cavitating flow in a real size transparent vco nozzle,” in
544 *Proceedings of the 22nd European conference on liquid atomization and*
545 *spray systems, ILASS, Como*, 2008. [https://doi.org/10.1017/jfm.](https://doi.org/10.1017/jfm.2013.32)
546 2013.32.
- 547 [19] A. Andriotis, M. Gavaises, and C. Arcoumanis, “Vortex flow and cavi-
548 tation in diesel injector nozzles,” *Journal of Fluid Mechanics*, vol. 610,
549 pp. 195–215, 2008. <https://doi.org/10.1017/S0022112008002668>.
- 550 [20] G. Sridhar and J. Katz, “Effect of entrained bubbles on the structure of
551 vortex rings,” *Journal of Fluid Mechanics*, vol. 397, pp. 171–202, 1999.
552 <https://doi.org/10.1017/S0022112099006187>.

- 553 [21] A. J. Cihonski, J. R. Finn, and S. V. Apte, “Volume displacement effects
554 during bubble entrainment in a travelling vortex ring,” *Journal of Fluid*
555 *Mechanics*, vol. 721, pp. 225–267, 2013.
- 556 [22] J. Choi and S. L. Ceccio, “Dynamics and noise emission of vortex cav-
557 itation bubbles,” *Journal of Fluid Mechanics*, vol. 575, pp. 1–26, 2007.
558 <https://doi.org/10.1017/S0022112006003776>.
- 559 [23] J. Choi, C.-T. Hsiao, G. Chahine, and S. Ceccio, “Growth, oscilla-
560 tion and collapse of vortex cavitation bubbles,” *Journal of Fluid Me-*
561 *chanics*, vol. 624, pp. 255–279, 2009. [https://doi.org/10.1017/](https://doi.org/10.1017/S0022112008005430)
562 [S0022112008005430](https://doi.org/10.1017/S0022112008005430).
- 563 [24] S. Dabiri, W. A. Sirignano, and D. D. Joseph, “Interaction between a
564 cavitation bubble and shear flow,” *Journal of Fluid Mechanics*, vol. 651,
565 pp. 93–116, 2010. <https://doi.org/10.1017/S0022112009994058>.
- 566 [25] M. Blessing, G. Konig, C. Kruger, U. Michels, and V. Schwarz, “Analysis
567 of flow and cavitation phenomena in diesel injection nozzles and its
568 effects on spray and mixture formation,” in *SAE 2003 World Congress &*
569 *Exhibition*, SAE International, mar 2003. [https://doi.org/10.4271/](https://doi.org/10.4271/2003-01-1358)
570 [2003-01-1358](https://doi.org/10.4271/2003-01-1358).
- 571 [26] M. Gavaises, D. Papoulias, A. Andriotis, E. Giannadakis, and
572 A. Theodorakakos, “Link between cavitation development and erosion
573 damage in diesel injector nozzles,” in *SAE World Congress & Ex-*

- 574 hibition, SAE International, apr 2007. [https://doi.org/10.4271/](https://doi.org/10.4271/2007-01-0246)
575 2007-01-0246.
- 576 [27] B. Reid, G. Hargrave, C. P. Garner, and G. Wigley, “An investigation
577 of string cavitation in a true-scale fuel injector flow geometry at high
578 pressure,” *Physics of Fluids*, vol. 22, 03 2010. [https://doi.org/10.](https://doi.org/10.1063/1.3372174)
579 1063/1.3372174.
- 580 [28] M. Gavaises, B. Reid, N. Mitroglou, G. Hargrave, C. Garner, E. Long,
581 and R. Mcdavid, “On the formation of string cavitation inside fuel in-
582 jectors,” *Experiments in Fluids*, vol. 55, 01 2014. [https://doi.org/](https://doi.org/10.1007/s00348-013-1662-8)
583 10.1007/s00348-013-1662-8.
- 584 [29] R. Lockett and A. Bonifacio, “Hydrodynamic luminescence in a model
585 diesel injector return valve,” *International Journal of Engine Research*,
586 07 2019. <https://doi.org/10.1177/1468087419870421>.
- 587 [30] L. Thimm, P. Trtik, H. Hansen, S. Jollet, and F. Dinkelacker, “Exper-
588 imental cavitation and spray measurement in real size diesel injection
589 nozzles with high resolution neutron imaging,” in *Proceedings of the 29th*
590 *Conference on Liquid Atomization and Spray Systems, ILASS Europe,*
591 *Paris*, 2019.
- 592 [31] M. McLorn, *Fundamental Behaviour of Valves Used in Diesel Fuel Injec-*
593 *tion Equipment*. PhD thesis, (Unpublished), City, University of London,
594 2013.

- 595 [32] N. Mitroglou, M. McLorn, M. Gavaises, C. Soteriou, and M. Winter-
 596 bourne, “Instantaneous and ensemble average cavitation structures in
 597 diesel micro-channel flow orifices,” *Fuel*, vol. 116, pp. 736 – 742, 2014.
 598 <https://doi.org/10.1016/j.fuel.2013.08.060>.
- 599 [33] M. Winterbourn, C. Soteriou, N. Mitroglou, M. Gavaises, and C. Dav-
 600 eau, “Visualising injection events in a fully operational diesel injector
 601 with a multi-hole transparent tip,” in *Thiesel, Valencia*, 2014.
- 602 [34] R. P. Fitzgerald, G. D. Vecchia, J. E. Peraza, and G. C. Martin, “Fea-
 603 tures of internal flow and spray for a multi-hole transparent diesel fuel
 604 injector tip,” in *29th Conference on Liquid Atomization and Spray Sys-*
 605 *tems, ILASS, Paris*, 2019.
- 606 [35] P. Koukouvinis, M. Gavaises, J. Li, and L. Wang, “Large eddy simulation
 607 of diesel injector including cavitation effects and correlation to erosion
 608 damage,” *Fuel*, vol. 175, pp. 26 – 39, 2016. [https://doi.org/10.1016/](https://doi.org/10.1016/j.fuel.2016.02.037)
 609 [j.fuel.2016.02.037](https://doi.org/10.1016/j.fuel.2016.02.037).
- 610 [36] A. Theodorakakos, G. Strotos, N. Mitroglou, C. Atkin, and M. Gavaises,
 611 “Friction-induced heating in nozzle hole micro-channels under extreme
 612 fuel pressurisation,” *Fuel*, vol. 123, pp. 143 – 150, 2014. [https://doi.](https://doi.org/10.1016/j.fuel.2014.01.050)
 613 [org/10.1016/j.fuel.2014.01.050](https://doi.org/10.1016/j.fuel.2014.01.050).
- 614 [37] G. Strotos, P. Koukouvinis, A. Theodorakakos, M. Gavaises, and
 615 G. Bergeles, “Transient heating effects in high pressure diesel injector

- nozzles,” *International Journal of Heat and Fluid Flow*, vol. 51, pp. 257
– 267, 2015. <https://doi.org/10.1016/j.ijheatfluidflow.2014.10.010>.
- [38] J. Shi, N. Guerrassi, G. Dober, K. Karimi, and Y. Meslem, “Complex physics modelling of diesel injector nozzle flow and spray supported by new experiments,” in *Thiesel, Valencia*, 2014.
- [39] J. Shi, P. Aguado Lopez, G. Dober, N. Guerrassi, W. Bauer, and M. Lai, “Using les and x-ray imaging to understand the influence of injection hole geometry on diesel spray formation,” in *Thiesel, Valencia*, 2016.
- [40] J. Shi, P. Aguado Lopez, E. Gomez Santos, N. Guerrassi, G. Dober, W. Bauer, M. Lai, and J. Wang, “Evidence of vortex driven primary breakup in high pressure fuel injection,” in *Proceedings of the 28th Conference on Liquid Atomization and Spray Systems, ILASS Europe, Valencia*, 2017. <http://dx.doi.org/10.4995/ILASS2017.2017.5707>.
- [41] J. Shi, P. Aguado Lopez, N. Guerrassi, and G. Dober, “Understanding high-pressure injection primary breakup by using large eddy simulation and x-ray spray imaging,” *MTZ worldwide*, vol. 78, pp. 50–57, 05 2017. <https://doi.org/10.1007/s38313-017-0039-4>.
- [42] J. Shi, P. Aguado Lopez, E. Gomez Santos, N. Guerrasi, W. Bauer, M.-C. Lai, and J. Wang, “High pressure diesel spray development: the effect of nozzle geometry and flow vortex dynamics,” in *Proceedings of*

- 637 *the 14th International Conference on Liquid Atomization and Spray Sys-*
638 *tems, ICLASS, Chicago, 2018.*
- 639 [43] M. Battistoni, Q. Xue, and S. Som, “Large-eddy simulation (les) of
640 spray transients: Start and end of injection phenomena,” *Oil Gas Sci.*
641 *Technol. - Rev. IFP Energies nouvelles*, vol. 71, no. 1, p. 4, 2016. [https:](https://doi.org/10.2516/ogst/2015024)
642 [//doi.org/10.2516/ogst/2015024](https://doi.org/10.2516/ogst/2015024).
- 643 [44] S. Bornschlegel, C. Conrad, A. Durst, J. Wang, and M. Wensing, “Multi-
644 hole gasoline direct injection: in-nozzle flow and primary breakup in-
645 vestigated in transparent nozzles and with x-ray,” *International Jour-*
646 *nal of Engine Research*, vol. 19, no. 1, pp. 67–77, 2018. [https:](https://doi.org/10.1177/1468087417746860)
647 [//doi.org/10.1177/1468087417746860](https://doi.org/10.1177/1468087417746860).
- 648 [45] F. Orley, S. Hickel, S. J. Schmidt, and N. A. Adams, “Large-eddy sim-
649 ulation of turbulent, cavitating fuel flow inside a 9-hole diesel injec-
650 tor including needle movement,” *International Journal of Engine Re-*
651 *search*, vol. 18, no. 3, pp. 195–211, 2017. [https://doi.org/10.1177/](https://doi.org/10.1177/1468087416643901)
652 [1468087416643901](https://doi.org/10.1177/1468087416643901).
- 653 [46] *ANSYS Fluent*, 2018.
- 654 [47] C. Brennen, *Cavitation and bubble dynamics*. Oxford: Oxford University
655 Press, 1995.
- 656 [48] P. J. Zwart, A. G. Gerber, and T. Belamri, “A two-phase flow model

- 657 for predicting cavitation dynamics,” in *Proceedings of the International*
658 *Conference on Multiphase Flow, ICMF, Yokohama, 2004.*
- 659 [49] P. Koukouvinis, H. Naseri, and M. Gavaises, “Performance of turbu-
660 lence and cavitation models in prediction of incipient and developed
661 cavitation,” *International Journal of Engine Research*, vol. 18, no. 4,
662 pp. 333–350, 2017. <https://doi.org/10.1177/1468087416658604>.
- 663 [50] S. B. Pope, *Turbulent Flows*. Cambridge University Press, 2000.
- 664 [51] F. Nicoud and F. Ducros, “Subgrid-scale stress modelling based on the
665 square of the velocity gradient tensor,” *Flow, Turbulence and Combustion*,
666 vol. 62, pp. 183–200, Sep 1999. [https://doi.org/10.1023/A:](https://doi.org/10.1023/A:1009995426001)
667 [1009995426001](https://doi.org/10.1023/A:1009995426001).
- 668 [52] E. H. I. Ndiaye, J.-P. Bazile, D. Nasri, C. Boned, and J. L. Daridon,
669 “High pressure thermophysical characterization of fuel used for testing
670 and calibrating diesel injection systems,” *Fuel*, vol. 98, pp. 288 – 294,
671 2012. <https://doi.org/10.1016/j.fuel.2012.04.005>.
- 672 [53] M. Chorazewski, F. Dergal, T. Sawaya, I. Mokbel, J.-P. E. Grolier, and
673 J. Jose, “Thermophysical properties of normafluid (iso 4113) over wide
674 pressure and temperature ranges,” *Fuel*, vol. 105, pp. 440 – 450, 2013.
675 <https://doi.org/10.1016/j.fuel.2012.05.059>.
- 676 [54] M. Gold, R. Pearson, J. Turner, D. Sykes, V. Stetsyuk, G. de Sercey,
677 C. Crua, F. Koukouvinis, and M. Gavaises, “Simulation and mea-

- 678 surement of transient fluid phenomena within diesel injection,” *SAE*
679 *Int. J. Adv. & Curr. Prac. in Mobility*, vol. 1, pp. 291–305, 01 2019.
680 <https://doi.org/10.4271/2019-01-0066>.
- 681 [55] E. Gomez Santos, J. Shi, W. Bauer, and M. Gavaises, “Modelling and
682 prediction of cavitation erosion in gasoline direct injection injectors oper-
683 ated with e100 fuel using a barotropic equation of state,” in *Proceedings*
684 *of the IMechE Fuel Systems Conference, London*, 2018.
- 685 [56] J. Shi, E. Gomez Santos, G. Hoffmann, and G. Dober, “Large eddy
686 simulation as an effective tool for gdi nozzle development,” *MTZ world-*
687 *wide*, vol. 79, pp. 58–63, Oct. 2018. [https://doi.org/10.1007/](https://doi.org/10.1007/s38313-018-0089-2)
688 [s38313-018-0089-2](https://doi.org/10.1007/s38313-018-0089-2).
- 689 [57] H. Tennekes and J. Lumley, *A First Course in Turbulence*. MIT Press,
690 1972.
- 691 [58] M. Battistoni, S. Som, and D. Longman, “Comparison of mixture and
692 multi-fluid models for in-nozzle cavitation prediction,” in *Proceedings of*
693 *ASME Internal Combustion Engine Division Fall Technical Conference,*
694 *ICEF, Dearborn*, 10 2013.
- 695 [59] J. P. V. Doormaal and G. D. Raithby, “Enhancements of the sim-
696 ple method for predicting incompressible fluid flows,” *Numerical Heat*
697 *Transfer*, vol. 7, no. 2, pp. 147–163, 1984. [https://doi.org/10.1080/](https://doi.org/10.1080/01495728408961817)
698 [01495728408961817](https://doi.org/10.1080/01495728408961817).

- 699 [60] J. Ferziger and M. Peric, *Computational Methods for Fluid Dynamics*.
700 Springer Berlin Heidelberg, 2012.
- 701 [61] B. Leonard, “The ultimate conservative difference scheme applied to un-
702 steady one-dimensional advection,” *Computer Methods in Applied Me-*
703 *chanics and Engineering*, vol. 88, no. 1, pp. 17 – 74, 1991. [https:](https://doi.org/10.1016/0045-7825(91)90232-U)
704 [//doi.org/10.1016/0045-7825\(91\)90232-U](https://doi.org/10.1016/0045-7825(91)90232-U).
- 705 [62] F. R. Menter, “Best practice: scale-resolving simulations in ansys cfd,”
706 in *ANSYS Technical report*, 2015.